VNU Journal of Science: Mathematics – Physics, Vol. 34, No. 2 (2018) 37-44

VNU Journal of Science: Mathematics - Physics

Journal homepage: https://js.vnu.edu.vn/MaP

Photoluminescence and Point Defect Related Emission of ZnO:Mn^{2+} micro/nanorod Fabricated by Co-precipitation Method

Nguyen Xuan Sang*, Le Phuoc Sang, Nguyen Minh Quan, Nguyen Huu Tho

Saigon University, 273 An Duong Vuong, Ward 3, District 5, Ho Chi Minh City, Vietnam

Received 29 May 2018
Accepted 15 July 2018

Abstract: Herein we study point defects and correlation to photoluminescence in ZnO nanorod. ZnO mirco/nanorod structure was successfully fabricated by co-precipitation method with highly homogeneous characteristics. When ion Mn^{+2} introduced into ZnO structure, the d-spacing distance of ZnO was increased from 0.248 nm to 0.295 nm due to the larger ionic radius of Mn^{2+} in comparison to Zn^{2+}. The photoluminescence emission evolution of ZnO through doping and annealing processes hinted the relation of point defect transformations. We found that zinc interstitial, zinc vacancy and its related defects were responsible mainly for photoluminescence emission in annealing and/or Mn^{2+} doped samples.

Keywords: ZnO nanorod, photoluminescence, co-precipitation, Mn^{2+} dopant, zinc vacancy

1. Introduction

Nowadays, one-dimensional (1D) micro/nanostructure ZnO fabrication and characterization have been attracted a lot of attention because of its highly potential application in light emitting device and the interesting unipolar property of the morphology which is suitable for gate-length miniaturization in semiconductor devices [1, 2]. Moreover, the morphological asymmetry may induce an advance in one-direction electron control which would bring high efficiencies in terms of electrical power, light emitting, and photocatalytic activity[2-5].

Recently, 1D ZnO crystals doped and undoped with transitional metal ions, such as Mn^{2+}, Cr^{3+}, Cu^{2+}, Fe^{2+} have been studied and showed interesting properties because the doped materials exhibited both semiconductor and magnetic behaviors [6-9]. For optical scheme, depending on treatment by thermal annealing or doped type, ZnO nanocrystals showed their emission profiles ranging from ultra-

*Corresponding author. Tel.: 84-904512337.
Email: sangxuannguyen@gmail.com
https//doi.org/ 10.25073/2588-1124/vnumap.4273

violet (UV) to intra-red (IR) emission which indicated its high application potential. The visible emission characteristics could be applied for light emitting technology, UV emission could be for UV detector[10], antibacterial systems by irradiation [11], and IR emission could be for telecommunication application [12]. Despite of the high potential application, the origins of optical property in doped and undoped semiconductors are still in debate because the results among different works showed different conclusions [13, 14] and the intrinsic defects induced photoluminescence emission are hard to define by experimentally extrapollation method.

In this work, we co-precipitately fabricated ZnO nanorod and studied photoluminescence emission evolution through annealing and Mn^{2+} doping treatments. Through emission profiles of these ZnO samples, we proposed point defect involved to emission in our samples. The study indicated that assigned defects, zinc interstitial (Zn_i), zinc vacancy (V_{Zn}) and radiative transition between singly and doubly ionized zinc vacancy ($V_{Zn}^{-} \leftrightarrow V_{Zn}^{--}$) were responsible to green emission at ~545 and ~570 nm, and red emission ~649 nm, respectively. Moreover, when ZnO was doped with ion Mn^{2+}, the atomic size difference between the doped ion and Zn^{2+}ion gave rise a structural deflection in the network that leaded the blue-shift in comparison to the free-standing ZnO.

2. Experimentals

The $Zn_{1-x}Mn_xO$ samples with x = 0.00 and 0.05 were prepared by co-precipitation method. The $Zn(CH_3COO)_2.2H_2O$ (Merck, ≥ 99%) was mixed with Hexamethylenetetramine (HMTA) (Merck, ≥99%) and the stoichiometrically corresponding amount of $Mn(CH_3COO)_2.4H_2O$ (Kanto, ≥ 99%)in 100 mL distilled water. Then, the resulted solution was added dropwise to 100 mL NaOH 2M (Merck, ≥ 99%) under vigorous stirring for 4h at room temperature (RT). The supernatant solution was then discarded carefully, the solid is washed with distilled water repeatedly until pH reached 7, and dried at 100^{o}C for an hour in air. Additionally, the powder were calcined for 4h in air at 450^{o}C for annealing process. The experimental conditions for the co-precipitation synthesis of samples S1 – S4 are given in Table 1.

Table 1. Sample information and experimental conditions for co-precipitation synthesis

Sample	$Zn(Ac)_2.2H_2O$ (in 100 mL)	NaOH (i100 mL)	Mn nominal concentration (at%.)	Annealing Temp/Time (^{o}C/h)
S1	0.1M	1M	0	
S2	0.1M	1M	0	450/4
S3	0.1M	1M	5	
S4	0.1M	1M	5	450/4

Structural investigations were performed with a Bruker D8 Advance X-ray diffractometer with CuKα radiation source (λ = 1.54064Å), sweep range 2θ of 20^o-70^o. Morphological properties was studied by Field Emission Scanning Electron Spectroscopy (FESEM, S4800 Hitachi). Optical bandgap were determined by UV-vis absorption measurement using UV-Vis spectrophotometry (HACH, DR5000). The optical emission characteristics were studied by room temperature photoluminescence measurement, using a 325-nm excitation wavelength analog spectrophotometer (Horiba, JobinYvon) equipped with a Xe lamp as an excitation source.

3. Result and discussions

3.1. Phase and structure

The undoped ZnO and Mn doped ZnO phases and structures were examined using X-ray diffraction analysis which also possibly identify foreign phases in the samples. Figure 1 showed the diffraction patterns of S1-S4 samples. The main diffraction peaks in the XRD patterns from S1 to S4 samples were indexed to the wurtzite structure (hexagonal) of ZnO, with lattice constants of a= 0.325 nm and c= 0.521 nm (JCPDS 36-1451 card)[7]. From S1 to S3 samples, there is no extra peaks related to impurity; however, the pattern of S4 sample exhibits further reflexes at 29.84° belonging to hetaerolite ($ZnMn_2O_4$) tetragonal secondary phase[15].

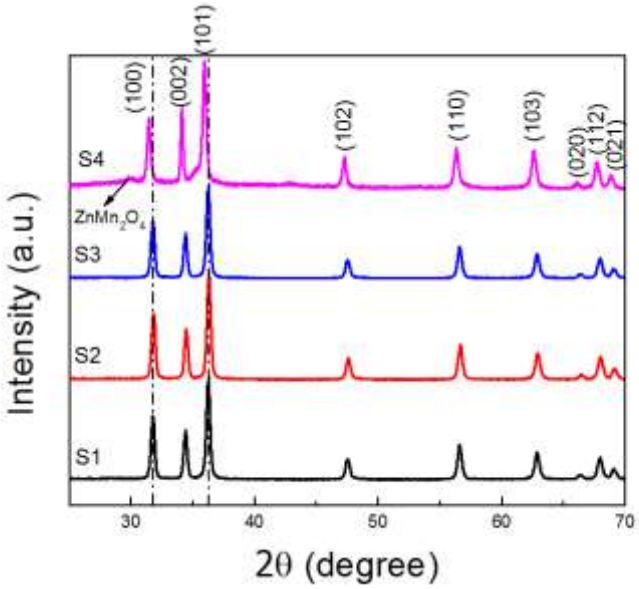

Figure 1. X-ray diffraction patterns of S1, S2, S3, and S4 samples

For further study, the doping and annealing processes' effects on the crystal growth, lattice parameters (a, and c), crystalline size and d-spacing distance should be clarified. The lattice parameters could be obtained by Bragg's law:

$$n\lambda = 2d\sin\theta \quad (1)$$

where n=1, λ is the wavelength of incident X-ray 0.15418 nm, and *d* is the spacing distance of two consecutive planes in the same direction. Then the following evaluation was defined for hexagonal phase:

$$\frac{1}{d^2} = \frac{4}{3}\left[\frac{h^2+hk+k^2}{a^2}\right] + \frac{l^2}{c^2} \quad (2)$$

where (hkl) are the Miller indexes.

The calculated result of d-spacing distances, lattice parameters and mean crystal sizes were showed in table 2. The d-spacing distances of S1, S2, and S3 samples were not changed with the value about 0.247 nm. It possibly indicated that ion Mn^{2+} was not diffuse further into the lattice. However, when annealed at 450°C, ions Mn^{2+} were introduced into the lattice as the result of d-spacing distance of S4 was increased to 0.295 nm. The increase could be understood that ion Mn2+ with the radius

(0.83 Å) was substituted for Zn2+ with a smaller radius (0.74 Å). The annealing process also increase mean crystal size of pure ZnO from ~22.4 nm to ~44.4 nm, and doped ZnO from 33.1 nm to 43.0 nm.

Table 2. The lattice parameters data of S1, S2, S3 and S4.

Sample	d_{101} (nm)	a (nm)	c (nm)	Crystal size (nm)
S1	0.248	0.325	0.521	22.40
S2	0.247	0.325	0.521	44.39
S3	0.247	0.325	0.520	33.11
S4	0.295	0.328	0.523	43.03

3.2. Morphology analysis

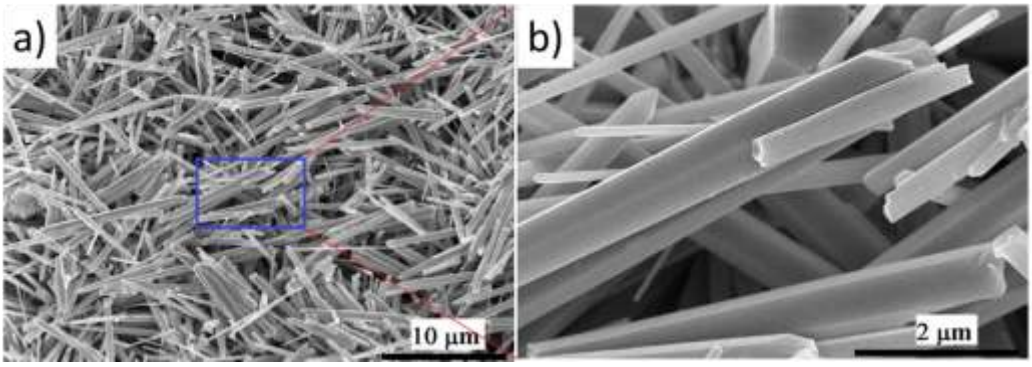

Figure 2. Scanning electron microscopic images of as-prepared ZnO.

Figure 2 showed the as-prepared ZnO sample with homogenous in diameter. The diameter and the length of a single ZnO rod are approximately 400 – 600 nm, ~10-20 µm, respectively. The diameter of these nano-structured gradually becomes smaller along the growth direction.The reaction mechanism of ZnO nanostructures can be formulated as followed:

$Zn^{2+} + 4OH^- \rightarrow Zn(OH)_4^{2-}$

$Zn(OH)_4^{2-} \rightarrow ZnO + 2H_2O + 2OH^-$

We assumed that the crystal formation process can be divided into two stages of nucleation and crystal growth.

3.3. Optical properties

In order to obtain a precise and quantifiable measure of the shifts in the band gaps from these absorption edges, we dissolved 0.004 (g) samples in 10 mL of ethanol (≥ 99%) under ultrasonic agitation for about 1h. Optical investigations were performed with DR 5000. The bandgap energy are calculated by equation: Eg = hc/λ, where h is Planck's constant, h = 6.625x10-34 J.s; c is the speed of light, c = 3x108 m.s-1 and λ is wavelength (nm).

Figure 3 shows the UV-absorption spectra of ZnO with different Mn concentrations, which are treated at mixed temperatures. Bandgap of bulk ZnO was 3.37 eV. The absorption edges of S1, S2, S3 and S4 are 3.34, 3.33, 3.38 and 3.33 eV, respectively. The position of S2's absorption spectra is almost the same in compare to S1. This indicates that annealing temperature does not affect the width of bandgap. The position of the absorption spectra is observed to shift towards the lower wavelength side with increasing Mn-doped concentrations in ZnO. This shows that the bandgap of the ZnO-based

material increases with the increase of ion Mn2+ concentration. Mn2+ has semi-saturated electron configuration (3d5), which trapped charge carriers from shallow donors. This leads to bandgap is extended (3.38 eV). When annealed at 450oC, bandgap is narrowed. We assumed that is because electrons are trapped by other intrinsic defects and merged with conduction band at room temperature.

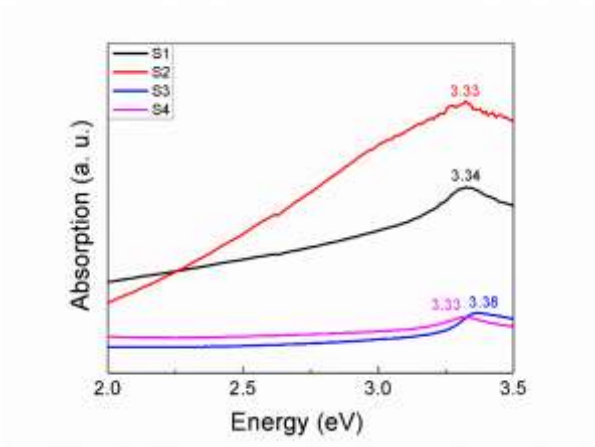

Figure 3. UV-vis absorption spectra of S1-S4 samples.

3.4. Photoluminescence (PL) study

3.4.1 Emission evolution of ZnO by thermal treatment

Photoluminescence (PL) is a suitable and nondestructive technique to determine the quality and the presence of impurities or defects in the materials. PL measurements were carried out at room temperature and the results of the Photoluminescence measurement on the mixed samples are presented in this section. In principle, the UV peak in the PL spectra is associated to the near band-to-band emission (NBE) while the visible emission originates from the defect levels, which includes zinc vacancies (V_{Zn}), interstitial zinc (Zn_i), interstitial oxygen (O_i) and lattice defects relating to oxygen and zinc.

Figure 4 illustrates the room temperature PL spectra of S1 and S2 samples. In addition to the no observations of NBE emission, these samples exhibit a broad intense deep-level (DL) emission appears in range of 500 – 900 nm. Upon annealing at 450oC, in general, the PL emission of S2 showed blue-shift after annealing treatment, from 700 nm in S1 to 600 nm in S2. Hence thermal treatment, in one hand, improved ZnO crystalline structure, and on the other hand, reduced point defects in asymmetrical sites, such as interstitial of Zn (Zn_i), and oxygen interstitial (O_i). The migration energy Zn_i was thermally unstable [13], then the application of temperature may expel Zn_i leaving zinc vacancy (V_{Zn}). However, oxygen related defect may introduced in the sample, i. e. oxygen interstitial near the surface. The DL emissions of these samples were Gaussian-resolved. According to Gaussian-fitted lines, visible peaks in each sample could be deconvoluted in to three peaks, in S1 sample, which centered at 634 nm (1.96 eV), 721 nm (1.72 eV) and 876 nm (1.42 eV) (Fig. 5a); while with one annealed at 450oC, S2, these are 569 nm (2.19 eV), 649 nm (1.91 eV) and 776 nm (1.6 eV) (Fig. 5b). In S1 sample, the emission centered at 634 nm (1.96 eV) was corresponded to excess local oxygen [4] and/or radiative transition between singly and doubly ionized VZn[3]while emission located at 721 nm (1.72 eV) is attributed to transitions from conduction band to Oi level [16]

and the peak at 876 nm (1.42 eV), was the trapping of charge carriers by O_i[10].The PL spectrum of S2 sample,which was annealed at 450^{o}C in air, showed three emission peaks which were blue-shifted in compare to the as-prepared one. Zinc vacancy may contribute to 569 nm (2.19 eV) emission, which was assigned to the transition from shallow donor to an acceptor of VZn, due to the low migration energy of zinc interstitial under annealing process [15-17]. The emission at 649 nm (1.91 eV) was assigned to radiative transition between singly and doubly ionized VZn and/or transitions from conduction band to Oi level [16]. In O-rich condition, the trapping of charge carriers by Oi, the radiative recombination of shallow donor and Oi as a trapped hole may give rise to the red emission at 776 nm (1.6 eV) [12].

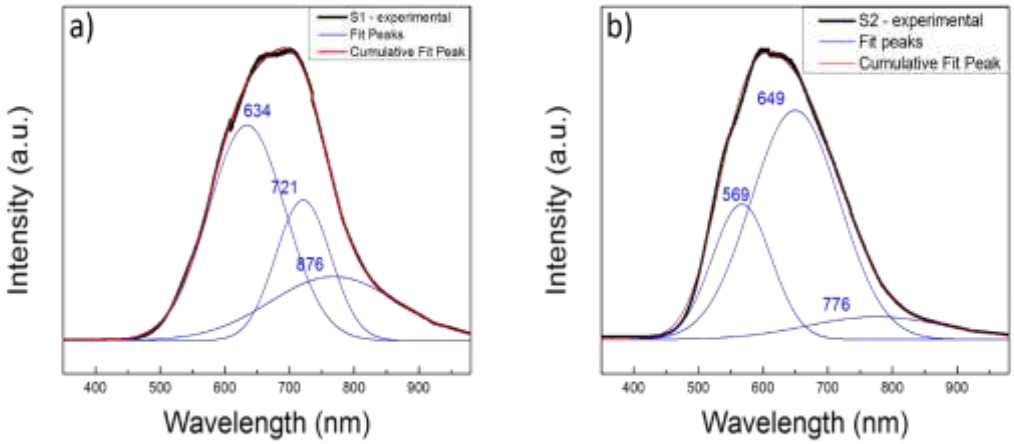

Figure 4. Photoluminescence spectra of: a)S1, b)S2.

3.4.2 Emission evolution of ZnO doped Mn^{2+} by thermal treatment

Figure 5 showed PL spectra of Mn doped ZnO at 5 at% nominal concentration of Mn^{2+} unannealed (S3) and annealed (S4) at450^{o}C for 4h in air.

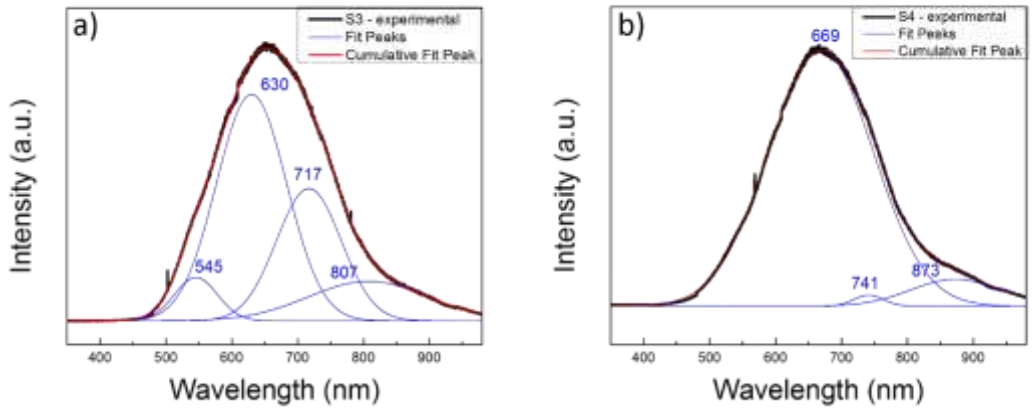

Figure 5. PLs spectra of: a) S3; b) S4.

When a certain amount of transition metal ion Mn2+ doped ZnO, the deep-level emission is changed. As-prepared Zn0.95Mn0.05O(S3) exhibited a spectral feature at 650 nm, its DL emission was Gaussian-resolved into four peaks at 545 nm (2.28 eV), 630 nm (1.97 eV), 717 nm (1.73 eV) and 887 nm (1.54 eV). The S4, sample annealed at 450oC, shows a peak centered at 667 nm. This was Gaussian-fitted into three peaks centered at 669 nm (1.86 eV), 741 nm (1.68 eV) and 873 nm (1.4 eV), in addition, which signal centered at 1.86 eV dominates the others.

In S3, as-prepared Zn0.95Mn0.05O, the peak centered at 545 nm (2.28 eV), according to Ramanachalam et al.[17], might be resulted from interstitial zinc (Zni). When introduced to ZnO, ions Mn2+ are likely to replace Zn2+ in the lattice, resulted in increasing Zni concentration. The other signals at 630 nm (1.97 eV), 717 nm (1.73 eV) and 887 nm (1.54 eV), are similar to which found in PL spectrum of S1. Since the ionic radius Mn2+ is larger than Zn2+, it causes a deflection in the network, leading to the small blue-shift in comparison to free-standing ZnO. For S4, Zn0.95Mn0.05O annealed at 450oC for 4 h in air, the Gaussian fit line peaks were at 669 nm (1.85 eV), 741 nm (1.67 eV) and 873 nm (1.42 eV), of them the signal centered at 1.85 eV dominates the others. Upon 450oC, the green emission (545 nm) was quenched. The quenching might due to Mni – Zni reactions [15] and/or competing defect reactions. The signal centered at 669 nm was possibly related to zinc defect, i. e. radiative transition between singly and doubly ionized VZn, similar to the dominated emission found in PL spectrum of S2 sample. When introduced ions Mn2+ in ZnO lattice, the unfilled electron states of transition ions may passivate oxygen related near the donor level. Hence, oxygen defect related radiative emissions were quenched.

4. Conclusions

We fabricated 1D ZnO micro/nanorod with homogenous size distribution (~400 nm in diameter, and ~15 μm in length) by co-precipitation method. The XRD spectra indicated ZnO samples in hexagonal wurtize structure and the d-spacing distance of Mn^{2+} doped ZnO with annealing treatment, 0.294 nm, is larger than that of the as-prepared sample, 0.247 nm. This result was attributed that Mn^{2+} was successfully doped in ZnO nanostructure. Photoluminescence study showed the defect evolution in ZnO under treatments and the defect transformation from zinc interstitial to zinc vacancy through annealing process. When doped with Mn^{2+} in crystal ZnO, the unfilled electrons in transitional ion could passivate electron traps in oxygen related defects and in conduction band which showed dominantly zinc vacancy related defect in PL emission.

Acknowledgement

This research is funded by Vietnam National Foundation for Science and Technology Development(NAFOSTED) under Grant Number 103.02-2016.87

References

[1] J. Miao, B. Liu, Part one: II–VI semiconductor nanowires, Semiconductor nanowire, Woodhead Publishing Series in Electronic and Optical Materials, (2015) 3-28.

[2] Y. Zhang, M.K. Ram, E.K. Stefanakos, D.Y. Goswami, Synthesis, Characterization, and Applications of ZnO Nanowires, Journal of Nanomaterials, 2012(2012) 1-22.

[3] M. Samadi, M. Zirak, A. Naseri, E. Khorashadizade, A.Z. Moshfegh, Recent progress on doped ZnO nanostructures for visible-light photocatalysis, Thin Solid Films, 605 (2016) 2-19.

[4] X. Zhang, J. Qin, Y. Xue, P. Yu, B. Zhang, L. Wang, R. Liu, Effect of aspect ratio and surface defects on the photocatalytic activity of ZnO nanorods, Scientific Report, 4 (2014) 4596.

[5] K.M. Lee, C.W. Lai, K.S. Ngai, J.C. Juan, Recent developments of zinc oxide based photocatalyst in water treatment technology: A review, Water Research, 88 (2016) 428-448.

[6] H. Harsono, I.N.G. Wardana, A.A. Sonief, Darminto, Crystallography, Impurities and Magnetic Properties of Mn-Doped ZnO Nanoparticles Prepared by Coprecipitation Method, Journal of Nano Research, 35 (2015) 67-76.

[7] X. Luo, W.T. Lee, G. Xing, N. Bao, A. Yonis, D. Chu, J. Lee, J. Ding, S. Li, J. Yi, Ferromagnetic ordering in Mn-doped ZnO nanoparticles, Nanoscale Res Lett, 9 (2014) 625.

[8] Y. Wang, J. Piao, Y. Lu, S. Li, J. Yi, Intrinsic ferromagnetism in Sm doped ZnO, Materials Research Bulletin, 83 (2016) 408-413.

[9] A. Savoyant, H. Alnoor, S. Bertaina, O. Nur, M. Willander, EPR investigation of pure and Co-doped ZnO oriented nanocrystals, Nanotechnology, 28 (2017) 035705.

[10] S. Singh, Y. Kumar, H. Kumar, S. Vyas, C. Periasamy, P. Chakrabarti, S. Jit, S.-H. Park, A study of hydrothermally grown ZnO nanorod-based metal-semiconductor-metal UV detectors on glass substrates, Nanomaterials and Nanotechnology, 7 (2017) 184798041770214.

[11] Z.H. Ibupoto, K. Khun, M. Eriksson, M. AlSalhi, M. Atif, A. Ansari, M. Willander, Hydrothermal Growth of Vertically Aligned ZnO Nanorods Using a Biocomposite Seed Layer of ZnO Nanoparticles, Materials (Basel), 6 (2013) 3584-3597.

[12] M. Wang, Y. Zhou, Y. Zhang, E. Jung Kim, S. Hong Hahn, S. Gie Seong, Near-infrared photoluminescence from ZnO, Applied Physics Letters, 100 (2012) 101906.

[13] A. Janotti, C.G. Van de Walle, Fundamentals of zinc oxide as a semiconductor, Reports on Progress in Physics, 72 (2009) 126501.

[14] A.B. Djurišić, Y.H. Leung, K.H. Tam, Y.F. Hsu, L. Ding, W.K. Ge, Y.C. Zhong, K.S. Wong, W.K. Chan, H.L. Tam, K.W. Cheah, W.M. Kwok, D.L. Phillips, Defect emissions in ZnO nanostructures, Nanotechnology, 18 (2007) 095702.

[15] S. Yildirimcan, K. Ocakoglu, S. Erat, F.M. Emen, S. Repp, E. Erdem, The effect of growing time and Mn concentration on the defect structure of ZnO nanocrystals: X-ray diffraction, infrared and EPR spectroscopy, RSC Advances, 6 (2016) 39511-39521.

[16] J. Lv, C. Li, Evidences of VO, VZn, and Oi defects as the green luminescence origins in ZnO, Applied Physics Letters, 103 (2013) 232114.

[17] M.S. Ramanachalam, A. Rohatgi, W.B. Carter, J.P. Schaffer, T.K. Gupta, Photoluminescence study of ZnO varistor stability, Journal of Electronic Materials, 24 (1995) 413-419.